Supplementary Information for Using Flory-Huggins-Informed Human-in-the-Loop Bayesian Optimization to Map the Phase Diagram of Polymer Blends

*Justin C. Hughes,[a] Dylan J. York,[b] Kevin G. Yager,[c] Chinedum O. Osuji,[b] Russell J. Composto[a]**

[a] Department of Materials Science and Engineering, University of Pennsylvania, Philadelphia, PA 19104, USA

[b] Department of Chemical and Biomolecular Engineering, University of Pennsylvania, Philadelphia, PA 19104, USA

[c] Center for Functional Nanomaterials, Brookhaven National Laboratory, Upton, NY 11973, USA

*Corresponding author

Calibration of Annealing Time using an Arrhenius Relation

Annealing times at each temperature were calibrated to achieve a comparable diffusion distance required for visibly detectable phase separation via cloud point measurement. Assuming an Arrhenius-type relation to describe polymer diffusion kinetics,[1] the required diffusion time τ to reach a sufficiently phase separated sample (for samples that would phase separate) is calculated using the proportionality in **Equation S1**, where E_{eff} is an effective free energy.

$$\tau \, \alpha \exp\left(\frac{-E_{eff}}{k_B T}\right) \tag{S1}$$

Times required for phase separation were measured at 0.5 wt. frac. PMMA for two different temperatures: 6 h at 170 °C and 0.33 h at 195 °C. Each was multiplied by a buffer factor of N = 1.5 (yielding 9 h and 0.5 h, respectively) to ensure complete phase separation. These two times were used to compute the temperature-dependent scaling implied by **Equation S1** and thereby determine the prescribed annealing duration for a desired target temperature. The implementation used in the experiment is provided in the Zenodo repository.

Calibration of Analysis Constants

All calibration data used in this section are provided in the *calibrations.csv* file in the Zenodo repository.

Calibration of Distance-Scaling Exponent (Equation 2)

Equation 2 includes a distance-scaling exponent of the form l_s^p to account for attenuation of illumination as a function of sample-to-light source distance. The exponent p was calibrated empirically by measuring illumination intensity I_m of otherwise identical samples at several distances r. The attenuation was fit using the expected power-law form in **Equation S2**.

$$I_m = I_o r^{-p} \tag{S2}$$

Taking the logarithm yields the linear relation in **Equation S3**.

$$\ln(I_m) = \ln(I_o) - p\ln(r) \tag{S3}$$

Linear regression of $\ln(I_m)$ versus $\ln(r)$ yielded p = 0.225, which was used in **Equation 2**.

Calibration of Transition Parameters (Equation 2)

After computing the background pixel intensity (I_B) and subtracting it from the average pixel intensity of the sample (I_S) and applying the distance-scaling factor $l_s^{0.225}$, two transition parameters h and k are leveraged to transform the argument to the hyperbolic tangent as shown in **Equation S4**.

$$Cloudiness = \frac{1}{2}[1 + tanh(h * ((I_S - I_B) * l_S^{0.225}) - k)] \tag{S4}$$

In this formulation, h controls how rapidly the cloudiness value rises as the contrast ($I_S - I_B$) increases, while k sets the contrast level at which the midpoint of the transition (Cloudiness = 0.5) occurs.

Both parameters were calibrated empirically by comparing the computed Cloudiness values to the visually observed appearance of a representative set of samples. The goal was to ensure that phase-separated films mapped close to 1, transparent films mapped close to 0, and intermediate cases varied smoothly between these extremes. This calibration yielded h = 0.015 and k = 80, which were used in **Equation 2**.

Calibration of Measurement Variance Scaling Factor (Equation 9)

In the Gaussian process surrogate, the noise covariance for an individual sample is taken to be proportional to the squared Cloudiness value, as reflected in the diagonal additive term in **Equation 9**. The corresponding total covariance matrix is shown in **Equation S5**, where the parameter a converts this proportionality to an equality.

$$K_{tot}(X, X) = K(X, X) + diag(a \cdot y_i^2) \tag{S5}$$

To calibrate a, Cloudiness measurements were repeated across identical samples under identical imaging conditions distributed across several (x,T) conditions spanning the range 0.25 – 0.75 wt. frac. PMMA and 155 – 175 °C. For each condition, an a value was computed using **Equation S6**, where V is the variance in Cloudiness value and m is the mean Cloudiness value across the repeat measurements.

$$a = \frac{V}{m^2} \tag{S6}$$

The resulting values ranged from effectively zero (for conditions producing samples with negligible contrast and negligible variance) up to approximately 0.03. To accommodate this spread and ensure stable inversion of the covariance matrix, a conservative estimation slightly above the maximum observed level was selected: a = 0.05, which was used in **Equation 9**.

Assembly Details for Custom Imaging Setup

A 3D rendering of the imaging setup is shown in **Figure S1**. The custom-milled panels were assembled using the integrated screw holes and fastening bolts. The camera was positioned over the circular opening on the top face so that its lens was centered, and it was secured using adhesive. The rectangular slit on the front face provided access for the halogen light source to illuminate the glass slide from the side, and the internal ridge ensured consistent slide positioning during imaging. After placing the silicon wafer and glass slide against the internal ridge, a cover panel was placed over the wide side opening before imaging. The full CAD model (STEP format) is available in the accompanying Zenodo repository.

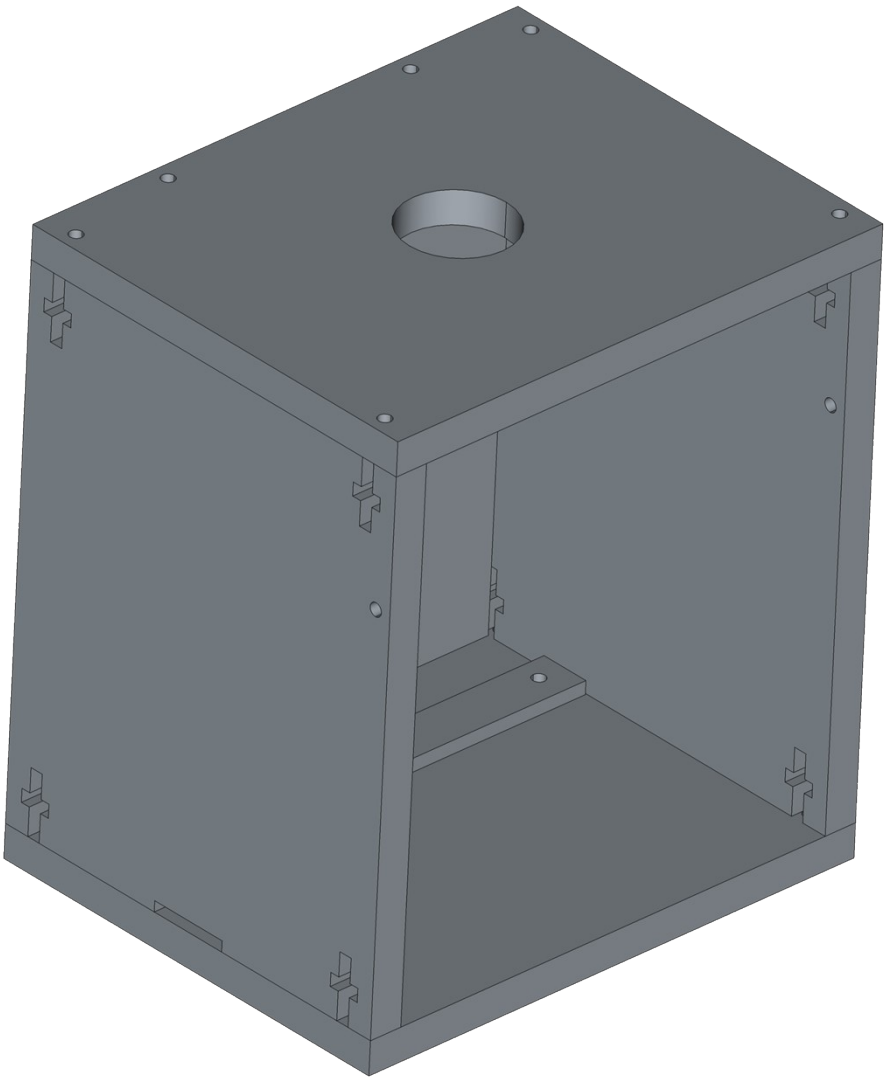

Figure S1. Rendered CAD model of imaging station showing circular opening for the camera on the top face, the rectangular slit for illumination on the front face, and the internal ridge for alignment.

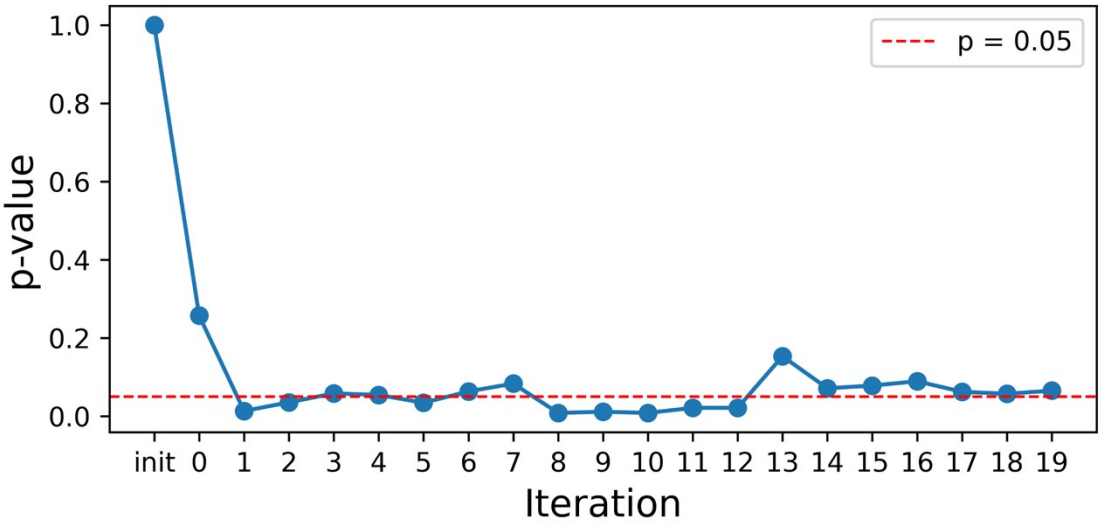

Figure S2. Mean p-values from Mann-Whitney U tests comparing posterior fields from the original (°C) and corrected (K) formulations. Only 8 of 21 iterations show $p < 0.05$; convergence of representations ($p > 0.05$) occurs by later iterations.

Mann-Whitney U Testing for Code Update

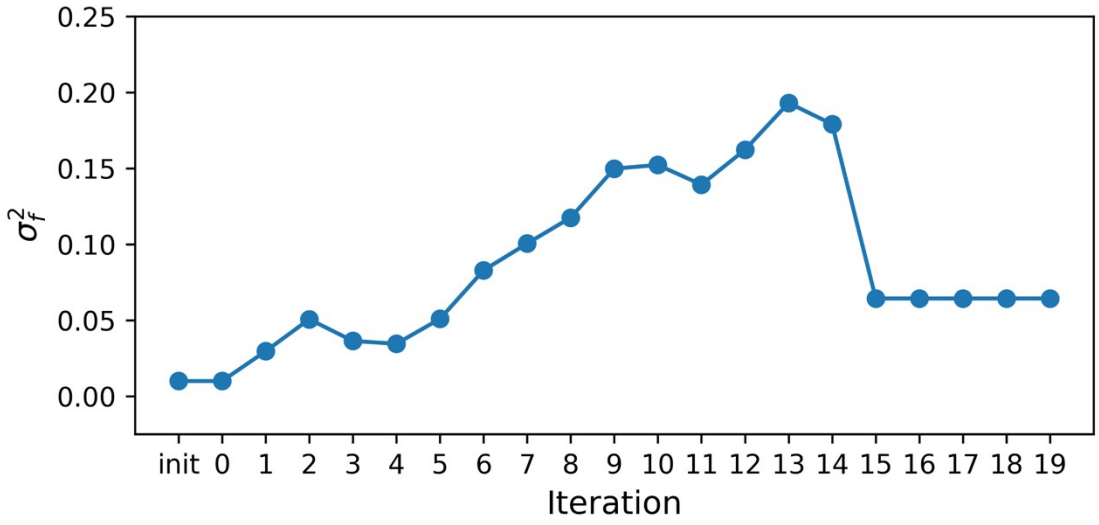

Figure S3. Hyperparameter log to visualize variation of noise hyperparameter (σ_f^2) over the course of the experimental campaign. Vertical axis limits are reduced relative to the boundaries established in **Table 1** to aid in visualizing early-iteration fluctuations and late-iteration stabilization.

Experimental Hyperparameter Log

Simulated Benchmarking of Flory-Huggins-Informed Mean and Kernel Approaches

To demonstrate the contribution of the Flory-Huggins-informed prior to algorithmic efficiency of the Bayesian optimization workflow, simulated experimental campaigns were conducted using the data from Newby *et al.*[2] as the ground truth. The same type of acquisition function, decision policy, and training approaches as described in **Materials and Methods** were employed for sake of comparison. For sake of computational efficiency, simulated campaigns used a smaller acquisition pool size (n_acq = 20) versus experiments (n_acq = 200). Three different simulated conditions were employed: (1) constant zero-prior mean with a Matérn-3/2 kernel, (2) Flory-Huggins-informed prior mean with a Matérn-3/2 kernel, and (3) constant zero-prior mean with a Flory-Huggins-augmented Matérn-3/2 kernel. The approach in (2) is identical to the surrogate modelling approach described in **Materials and Methods**. The kernel augmentation in (3) is displayed below in **Equation S7**, where the Flory-Huggins interaction parameter enters as another term in the kernel formulation.

$$r_{aug}(x, x') = \sqrt{\left(\frac{x - x'}{l_x}\right)^2 + \left(\frac{T - T'}{l_T}\right)^2 + \left(\frac{\chi - \chi'}{l_\chi}\right)^2} \tag{S7}$$

This scaled interpoint distance still enters **Equation 6** to calculate the kernel value between two points. This specific formulation was designed to encapsulate physical theory in a different part of the workflow than the Flory-Huggins-informed prior mean. Aside from residing in a different part of the surrogate modelling process, the other major difference between this and the approach in the paper is that the values of A and B required to compute the Flory-Huggins interaction parameter χ (according to **Equation 3**) is that the A and B values were fixed. The Flory-Huggins parameters A and B were fixed at values of 0.0217 and -8.2186, respectively, corresponding to the final estimates from the experimental campaign in the main text. Holding these parameters fixed isolates the effect of kernel-based physics integration and distinguishes it from the prior-mean-based approach where A and B were treated as trainable parameters.

The simulated experimental campaigns used convergence of hyperparameters as the convergence condition to terminate the experimental campaign. The initial values and ranges of hyperparameters used for the simulations are displayed in **Table S1** below.

Simulation Condition	**Hyperparameter**	**Initial Value**	**Lower Bound**	**Upper Bound**
Zero-prior mean	Noise (σ_f^2)	0.1	0.01	100
	Composition length scale (l_x)	0.01	0.001	1
	Temperature length scale (l_T)	1	0.1	100

Flory-Huggins-informed prior	Noise (σ_f^2)	0.1	0.01	100
	Composition length scale (l_x)	0.01	0.001	1
	Temperature length scale (l_T)	1	0.1	100
	Flory-Huggins Parameter A	0	-1	1
	Flory-Huggins Parameter B	0	-200	200
Flory-Huggins-augmented kernel	Noise (σ_f^2)	0.1	0.01	100
	Composition length scale (l_x)	0.01	0.001	1
	Temperature length scale (l_T)	1	0.1	100
	χ length scale (l_χ)	0.001	0.000001	0.1

Table S1. Initial values and boundaries for kernel and structured prior hyperparameters over the different simulation conditions.

The noise, composition length scale, and temperature length scale initial values and boundaries are shared among the different simulation conditions for sake of comparison between the different conditions. These hyperparameter initial values and boundaries were used over 50 simulated experimental campaigns per condition, and the results from each campaign were aggregated in **Table S2** below to display the mean and standard deviation of iterations required for hyperparameter convergence per condition.

Simulation Condition	**Mean Iterations to Convergence**	**Standard Deviation (Iterations)**
Zero-prior mean	29.32	4.38
Flory-Huggins-informed prior	23.26	7.24
Flory-Huggins-augmented kernel	27.74	4.89

Table S2. Mean and standard deviation of number of iterations required for hyperparameter convergence across 50 simulated campaigns for each simulation condition.

Under the same simulation budget and equivalent parameterizations (excluding the limited prior and kernel structures varied for comparison), the Flory-Huggins-informed prior consistently converged in fewer iterations on average than either a zero-mean prior or a Flory-Huggins-augmented kernel. This suggests that embedding physics in the prior mean improves algorithmic efficiency over a baseline zero-mean prior formulation and is more effective than incorporating fixed physical information through the kernel alone.

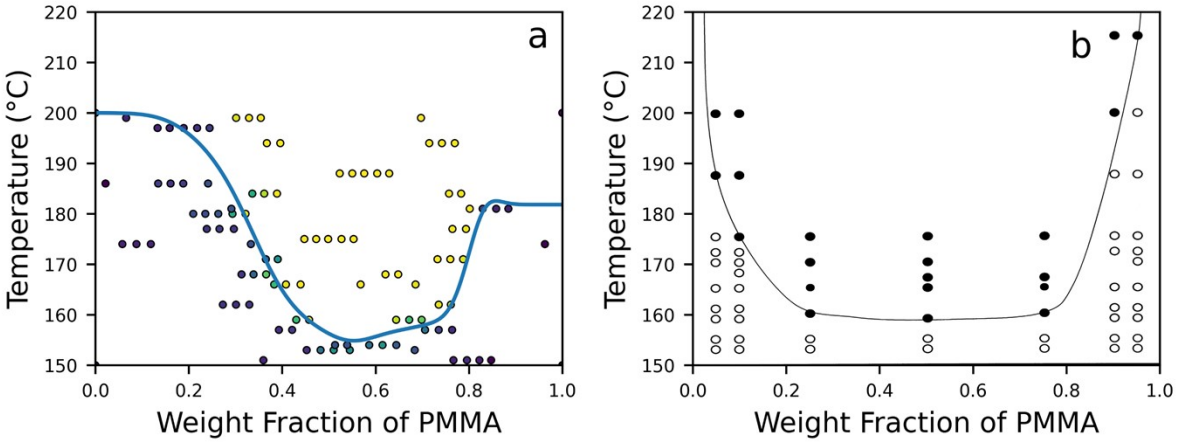

Figure S4. Visual comparison of phase boundary generated from a) this study and b) the reference study from Newby *et al.*[2]

Phase Boundary Comparison to Literature Phase Diagram

Numerical Comparison of Calculated Interaction Parameter with Literature Values

Source	Value	A	B (K)	χ(T = 160 °C)
This work	Calculated χ	0.0217	-8.2186	0.002726
	χ_C (Flory-Huggins)	----------	----------	0.002678
Previous literature[3]	Calculated χ	0.5357	-237.4743	-0.01254

Table S3. Comparison of the Flory-Huggins interaction parameters evaluated at the literature-reported[2] LCST of 160 °C with the corresponding critical Flory-Huggins interaction parameter.

Table S3 compares the interaction parameter computed from the fitted A and B values from this work with values constructed from literature-reported[3] segmental interaction parameters, evaluated at the reported[2] LCST of 160 °C. This comparison shows that the interaction parameter calculated from the A and B values fit in this work closely match the corresponding Flory-Huggins critical interaction parameter (**Equation S8**), where N_{PMMA} and N_{SAN} are the degrees of polymerization of PMMA and SAN used in this work respectively.

$$\chi_C = \frac{1}{2}\left(\frac{1}{\sqrt{N_{PMMA}}} + \frac{1}{\sqrt{N_{SAN}}}\right)^2 \quad \text{(S8)}$$

In contrast, a χ value calculated using copolymer mixing rules does not satisfy that condition. While this does not diminish the value of copolymer mixing rules, it demonstrates that the experimental phase boundary can be captured using a simpler Flory-Huggins framework.

References

(1) Gennes, P.-G. de. *Scaling Concepts in Polymer Physics*; Cornell university press: Ithaca (N.Y.) London, 1991.

(2) Newby, B. Z.; Composto, R. J. Influence of Lateral Confinement on Phase Separation in Thin Film Polymer Blends. *Macromolecules* **2000**, *33* (9), 3274–3282. https://doi.org/10.1021/ma992092m.

(3) Higashida, N.; Kressler, J.; Inoue, T. Lower Critical Solution Temperature and Upper Critical Solution Temperature Phase Behaviour in Random Copolymer Blends: Poly(Styrene-*Co*-Acrylonitrile)/Poly(Methyl Methacrylate) and Poly(Styrene-*Co*-Acrylonitrile)/Poly(ε-Caprolactone). *Polymer* **1995**, *36* (14), 2761–2764. https://doi.org/10.1016/0032-3861(95)93654-5.